COMMUNICATION

Selective Electrocatalysis of Nitrous Oxide Reduction Reaction to Nitrogen at Carbon-Supported Pt–Pd–Sn Nanoparticles

Received 00th January 20xx,
Accepted 00th January 20xx

DOI: 10.1039/x0xx00000x

Abinash Chandro Sarker,†[a] Masaru Kato,*[a,b] Mitsuki Kawamura,[a] Takeshi Watanabe,[c] and Ichizo Yagi*[a,b]

Nitrous oxide (N_2O) is the third-largest greenhouse gas and must be removed using a green method at ambient conditions, such as electrocatalysis. Here, we report carbon-supported Pt–Pd–Sn nanoparticles (Pt–Pd–Sn/C) for electrocatalytic N_2O reduction reaction (N_2ORR) to N_2 in acidic media. Pt–Pd–Sn/C shows about 100% Faradaic efficiency for the N_2ORR to N_2 at ≥+0.06 V vs. RHE. Pt–Pd–Sn/C also shows high N_2ORR selectivity to N_2 in the presence of O_2: about 44% Faradaic efficiency at a 1:10 N_2O–O_2 molar ratio. Pt–Pd–Sn/C has Sn oxide or hydroxide patches on Pt–Pd nanoparticles. The PtPd/Sn interface can work as the catalytic active site.

Nitrous oxide (N_2O) is the third-largest greenhouse gas with about 300 times greater global warming potential than CO_2 and is also responsible for ozone depletion.[1–6] N_2O is mainly released from agricultural sources: fertilizers, manures, and crop residues as a by-product of biological denitrification processes ($NO_3^- \rightarrow NO_2^- \rightarrow NO \rightarrow N_2O \rightarrow N_2$).[7] Combustion of fossil fuels, biomass burning, and industrial activities such as nitric acid, adipic acid, and caprolactam production plants are also accountable for increasing the concentration of N_2O in the atmosphere.[3,8] The concentration of N_2O is about 337 ppb till January 2024, with an increasing rate of about 1 ppb annually.[9] Therefore, there is an urgent need to develop efficient technologies that can remove N_2O in an environmentally friendly way.

Several technologies have been developed for N_2O removal: thermal decomposition, direct catalytic decomposition, selective catalytic reduction, and electrocatalytic reduction.[10–14] Thermal decomposition and direct catalytic decomposition require harsh conditions at very high (>1073 K) and medium temperatures (573–773 K), respectively.[10,12,13] Selective catalytic reduction requires reducing agents like propane/ammonia.[11,12] In contrast, the electrocatalytic N_2O reduction reaction (N_2ORR) can reduce N_2O to N_2 or ammonia with no reducing agent under ambient conditions at room temperature and atmospheric pressure.[15,16] As N_2ORR electrocatalysts, noble metals, including Pt and Pd, have been studied.[14,17–21] For example, Pd-based nanoparticles (NPs) supported on carbon black[5] or fluorine-doped tin oxide[22] have been reported. In the latter case, the interaction between the noble metal and the Sn-containing substrate enhances the N_2ORR activity. Sn is known to suppress hydrogen adsorption to the surface of noble metals and thereby enhance the electrocatalytic reduction of NO_3^- and N_2O.[16,22–25] Thus, electrocatalysts featuring the interface of noble metals such as Pd with Sn can show high activity for the N_2ORR.

Herein, we report the electrocatalytic N_2ORR activity and selectivity to N_2 for carbon-supported Pt–Sn and Pt–Pd–Sn NPs in acidic media (**Fig. 1**). To evaluate the catalytic activity and selectivity, turnover frequencies (TOFs) and Faradaic efficiencies (FEs) for the N_2ORR to N_2 were determined. We also perform the N_2ORR electrocatalysis using Pt–Pd–Sn NPs in the presence of O_2 to obtain the design concept of N_2ORR selective catalysts for practical use because the molar ratio of N_2O:O_2 in the atmosphere is 1:(6.2×10^5).[9,26]

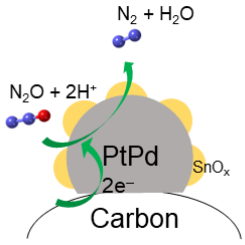

Fig. 1 Schematic representation of the electrocatalytic N_2ORR on Pt–Pd–Sn/C in acidic media.

[a] *Graduate School of Environmental Science, Hokkaido University, N10W5, Kita-ku, Sapporo 060-0810, Japan*
[b] *Faculty of Environmental Earth Science, Hokkaido University, N10W5, Kita-ku, Sapporo 060-0810, Japan*
[c] *Industrial Application and Partnership Division, Japan Synchrotron Radiation Research Institute (JASRI), SPring-8, 1-1-1 Kouto, Sayo 679-5198, Japan*
*Corresponding authors: masaru.kato@ees.hokudai.ac.jp (MK), iyagi@ees.hokudai.ac.jp (IY)
† Present Address: Department of Chemistry, Begum Rokeya University, Rangpur, Rangpur 5404, Bangladesh.
Electronic Supplementary Information (ESI) available: See DOI: 10.1039/x0xx00000x

Pt–Pd–Sn NPs were synthesized from the mixture of [Pt(acac)$_2$] (acac = acetylacetonato), [Pd(acac)$_2$], and $SnCl_2 \cdot 2H_2O$ as metal precursors and a borane-morpholine complex as a reductant in oleylamine after heating at three stages: 333, 363, and 453 K under Ar and then immobilized on a carbon black of Vulcan XC-72R (Pt–Pd–Sn/C; see the detail in the Supporting Information, SI). As a control sample, carbon-supported Pt–Sn NPs were also synthesized in the similar synthetic procedure (Pt–Sn/C; see the detail in the SI).

Transmission electron microscopy (TEM) images of Pt–Pd–Sn/C showed the presence of NPs with an average size of 10.2±3.0 nm on the carbon support (**Fig. 2a and S2**). High-angle annular dark field-scanning transmission electron microscopy (HAADF-STEM) and energy dispersive spectroscopy (EDS) mapping images of Pt–Pd–Sn/C confirmed the Sn patches around Pt-Pd mixture NPs with a Pt:Pd:Sn atomic ratio of 52:29:19 (**Fig. 2b and 2c**), which is almost the same as the ratio of 48:29:23 obtained from inductively coupled plasma mass spectroscopy (ICP-MS) measurements. For Pt–Sn/C, TEM, HAADF-STEM, and EDS mapping images also revealed the Sn-patched Pt NPs with a Pt:Sn atomic ratio of 81:19 (**Fig. S3**), which is the same as that obtained from ICP-MS measurements. The average size of the Pt–Sn NPs was found to be 8.2±2.1 nm. X-ray powder diffraction (XRD) patterns of the Pt–Pd–Sn/C and Pt–Sn/C indicate the representative face-centered cubic structure (**Fig. S4** and **Table S1**).[27,28]

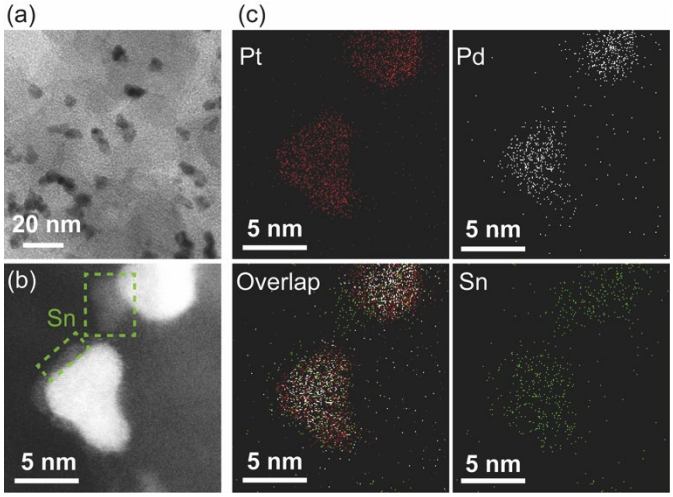

Fig. 2 (a) TEM, (b) HAADF-STEM, and (c) EDS elemental mapping images of Pt–Pd–Sn/C. The red, pale white, and green dots indicate the Pt, Pd, and Sn elements, respectively.

X-ray photoelectron spectroscopy (XPS) data in the Sn 3d region confirm the presence of Sn^{2+} and Sn^{4+} species for Pt–Pd–Sn/C and Pt–Sn/C (**Fig. S5**). It was also supported by Sn *K*-edge X-ray absorption spectroscopy (XAS) data (**Fig. S6**). For Pt and Pd elements, metallic species are dominant in both Pt–Pd–Sn/C and Pt–Sn/C, as confirmed by XPS in the Pt 4f and Pd 3d regions (**Fig. S5**). Based on these results and HAADF-STEM and EDS mapping images as mentioned above (**Fig. 2**), tin oxide or hydroxide species such as SnO_2, SnO or $Sn(OH)_2$ are placed as patches on metallic Pt–Pd nanoparticles for Pt–Pd–Sn/C. Curve fit analysis of Fourier transforms of extended X-ray absorption fine structure oscillations (**Fig. S7**) allows us to determine the bond lengths of Sn-O to be 2.03±0.01 Å for Pt–Pd–Sn/C and 2.06±0.01 Å for Pt–Sn/C (**Table S2**).

To understand the redox behavior of Sn species, cyclic voltammograms (CVs) of Pt–Pd–Sn/C and Pt–Sn/C were recorded at a sweep rate of 50 mV s^{-1} in a 0.1 M $HClO_4$ aqueous solution under an inert condition of Ar (**Fig. S8**). Hydrogen adsorption/desorption currents were observed in the potential range between +0.06 and +0.36 V vs. RHE. In the positive-going sweep, Sn oxidation waves were observed between +0.6 and +0.9 V vs. RHE. No such wave was observed for Pt–Pd/C and Pt/C. In the negative-going sweep, wider reduction peaks of metal oxides or hydroxide between +0.54 and +0.70 V vs. RHE for Pt–Pd–Sn/C and Pt–Sn/C were observed than those of Pt–Pd/C and Pt/C.[29] These results indicate that Sn species are redox-active on the surface of Pt–Pd NPs for Pt–Pd–Sn/C. Under the N_2O-saturated condition, CVs of the Pt–Pd–Sn/C and Pt–Sn/C showed cathodic currents in the potential range between +0.06 and +0.36 V vs. RHE (**Fig. 3a**). These currents are associated with the electrochemical N_2ORR.[22,30] The Pt–Pd–Sn/C showed higher N_2ORR current density than the Pt–Sn/C did (**Fig. 3a**). The N_2ORR current density of –0.57 mA cm^{-2} at +0.16 V vs. RHE for Pt–Pd–Sn/C is about two times higher than that of –0.27 mA cm^{-2} for Pt–Sn/C (**Fig. 3b**). Thus, the trimetallic Pt–Pd–Sn/C catalyst is more active than the bimetallic Pt–Sn/C catalyst, which is in good agreement with our previous electrocatalysts of Pt and Pd NPs on fluorine-doped tin oxide (Pt/Pd/FTO and Pt/FTO).[22] The value of the N_2ORR current density of Pt–Pd–Sn/C at +0.16 V vs. RHE **(Fig. 3b)** was about two times higher than –0.25 mA cm^{-2} of the Pt/Pd/FTO electrode.[22]

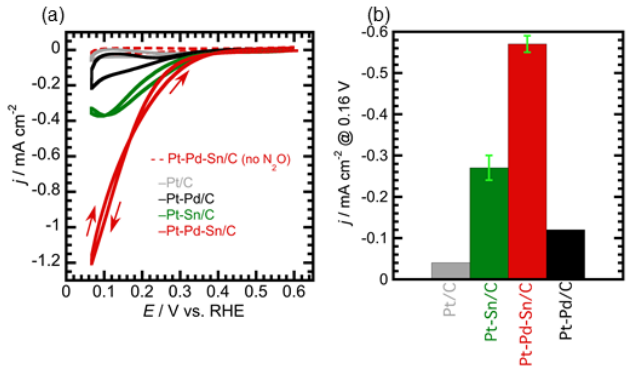

Fig. 3 CVs of Pt–Pd–Sn/C, Pt–Sn/C, Pt–Pd/C, and Pt/C in a 0.1 M $HClO_4$ aqueous solution (a) at a sweep rate of 10 mV s^{-1} under N_2O in the absence of O_2. (b) Current densities of the catalysts at +0.16 V vs. RHE for the N_2ORR.

The N_2ORR activity of the catalysts used in this work is in the following order: Pt–Pd–Sn/C > Pt–Sn/C > Pt–Pd/C > Pt/C. Because Pt–Pd/C and Pt/C showed much lower N_2ORR activity at +0.16 V vs. RHE than Pt–Pd–Sn/C and Pt–Sn/C, respectively (**Fig. 3b**), the presence of Sn species drastically enhances the electrocatalytic N_2ORR activity. In the potential region between +0.06 and +0.36 V vs. RHE, the adsorption of N_2O competes with the adsorption of hydrogen (**Fig. S8**).[18,20,21] The Sn/PtPd interface could enhance the adsorption of N_2O and/or suppress the adsorption of hydrogen, leading to the enhancement of the N_2ORR activity.[22,24] The modulation of the N_2O adsorption can be supported by the charge transfer from Sn to Pt and Pd in XPS of Pt–Pd–Sn/C: lower binding energy shifts of Pt–Pd–Sn/C than Pt–Pd/C in the Pt 4f and Pd 3d regions (**Fig. S5a** and **S5b**).

The product analysis of Pt–Pd–Sn/C for the N_2ORR using gas chromatography equipped with a thermal conductivity detector reveals almost 100% FE to N_2 at ≥+0.06 V vs. RHE. Chronoamperometric experiments of Pt–Pd–Sn/C and Pt–Sn/C were

performed in a 0.1 M $HClO_4$ aqueous solution under N_2O at three equidistant potentials: 0, +0.06, and +0.12 V vs. RHE for 1 h (**Fig. S9**). The Pt–Pd–Sn/C and Pt–Sn/C showed almost 100% FE for N_2 at +0.06 and +0.12 V vs. RHE, whereas the FE of N_2 decreased at 0 V vs. RHE due to the hydrogen evolution reaction (**Fig. 4a** and **4b**, and **Table S3**).[14] At 0 V vs. RHE, the FEs of N_2 and H_2 at Pt–Pd–Sn/C were found to be about 75 and 11%, respectively, whereas about 64 and 30%, respectively, at Pt–Sn/C. The lower value of the FE to H_2 at Pt–Pd–Sn/C than that at Pt–Sn/C indicates that the trimetallic Pt–Pd–Sn/C catalyst is more selective to the N_2ORR over the hydrogen evolution reaction than the bimetallic Pt–Sn/C catalyst.

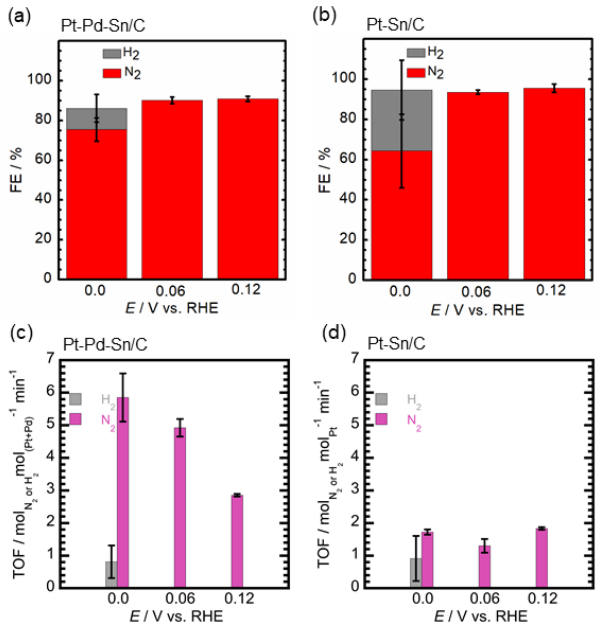

Fig. 4 FEs of N_2 and H_2 at (a) Pt–Pd–Sn/C and (b) Pt–Sn/C, and TOFs of N_2 and H_2 at (c) Pt–Pd–Sn/C and (d) Pt–Sn/C obtained from N_2ORR in a 0.1 M $HClO_4$ aqueous solution under N_2O in the absence of O_2 after 1 h electrolysis at 0, +0.06, and +0.12 V vs. RHE at room temperature and atmospheric pressure.

A TOF of Pt–Pd–Sn/C at +0.06 V vs. RHE for the N_2ORR to N_2 was determined to be 4.92±0.27 mol_{N2} $(mol_{Pt+Pd})^{-1}$ min^{-1} (**Fig. 4c** and **Table S4**). This is about three times higher than that of 1.30±0.21 mol_{N2} $(mol_{Pt})^{-1}$ min^{-1} for Pt–Sn/C (**Fig. 4d** and **Table S4**), about 82 times greater than that of Pd foil at +0.1 V vs. RHE, and about 11 times higher than that on Au@Pd core@shell nanoparticle electrode at –0.4 V vs. SCE (+0.64 V vs. RHE), calculated from previously published data.[5,31]

The high FEs and TOFs of Pt–Pd–Sn/C for the N_2ORR to N_2 encouraged us to investigate the Pt–Pd–Sn/C for the electrocatalytic N_2ORR selectivity in the presence of O_2. In the N_2O–O_2 mixture with a 1:1 molar ratio of N_2O to O_2, a FE of 71% for the N_2ORR to N_2 retains at +0.06 V vs. RHE (**Fig. 5** and **Table S5**), and therefore Pt–Pd–Sn/C is N_2ORR selective compared to O_2. Even at an O_2-rich 1:10 molar ratio of N_2O to O_2, a FE of 44% was obtained. TOFs of Pt–Pd–Sn/C at +0.06 V vs. RHE for the N_2ORR to N_2 in the N_2O–O_2 mixture with 1:1 and 1:10 N_2O–O_2 ratios were determined to be 2.14±0.02 and 0.52±0.02 mol_{N2} $(mol_{Pt+Pd})^{-1}$ min^{-1}, respectively (**Fig. S10** and **Table S5**). Because Pt and Pd efficiently catalyze the oxygen reduction reaction (ORR),[32,33] one of the possible explanations is that Sn oxide or hydroxide patches on the catalyst surface can block the access of O_2 to the surface, resulting in the selective N_2ORR to N_2. Another possible explanation is the difference in solubility between N_2O and O_2 in water: 24 mM for N_2O and 1.3 mM for O_2 at 298.15 K.[34,35] Further experimental studies will be required to understand the mechanistic insight into the N_2ORR selectivity of Pt–Pd–Sn/C over the ORR.

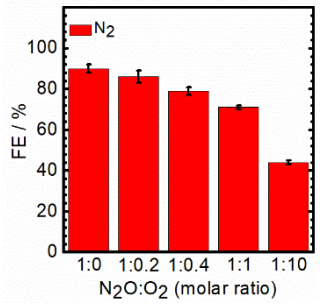

Fig. 5 FEs of N_2 obtained from N_2ORR in a 0.1 M $HClO_4$ aqueous solution under different molar ratios of the N_2O–O_2 mixture at Pt–Pd–Sn/C at +0.06 vs. RHE at room temperature and atmospheric pressure.

Conclusions

In conclusions, Pt–Pd–Sn/C exhibits high electrocatalytic N_2ORR activity and selectivity to N_2 in acidic media. The Sn oxide or hydroxide at the surface increases the adsorption of N_2O and/or suppresses the adsorption of hydrogen, resulting in the higher electrocatalytic N_2ORR activity than the bimetallic Pt–Sn/C catalyst. Pt–Pd–Sn/C shows about 100% FE for the N_2ORR to N_2 at ≥+0.06 V vs. RHE under N_2O in the absence of O_2. Under 1:1 N_2O–O_2 molar ratio, the FE of 71% is observed for Pt–Pd–Sn/C, where possibly the Sn species block the access or adsorption of O_2 at the Pt or Pd surface, which can catalyze the ORR. Our results will provide design concepts for the development of highly efficient N_2ORR electrocatalysts and O_2-tolerant electrocatalysts for the removal of N_2O from air.

Author Contributions

Abinash Chandro Sarker performed the synthesis, characterization and electrocatalysis. Masaru Kato and Ichizo Yagi conceptualized and supervised the project. Mitsuki Kawamura and Takeshi Watanabe helped XAS measurements. The manuscript was written through the contributions of all authors. All authors wrote, commented on, and approved the final version of the manuscript.

Conflicts of interest

The authors declare no competing financial interest.

Data availability

The data supporting this article have been included as part of the Supplementary Information.

Acknowledgements

The authors thank Professor Shinichiro Noro (Faculty of Environmental Earth Science, Hokkaido University) for giving XRD facilities; Takashi Tanioka and Ryoko Yokohira (Faculty of Engineering, Hokkaido University) for taking TEM images; Naomi Hirai and Yuko Mori (Research Institute for Electronic Science, Hokkaido University) for taking the HAADF-STEM and EDS mapping images, and XPS data; Nozomi Takeda (Open Facility Division, Hokkaido University) for ICP-MS measurements. This work was financially supported by the Ministry of Education, Culture, Sports, Science and Technology (MEXT), the "Nanotechnology Platform" program of the MEXT for Hokkaido University (JPMXP09A18HK0063, 19HK0030 and 21HK0062). The synchrotron radiation experiments were performed at the BL14B2 of SPring-8 with the approval of the Japan Synchrotron Radiation Research Institute (JASRI) (Proposal No. 2022B0608).

References

1 H. Tian, R. Xu, J. G. Canadell, R. L. Thompson, W. Winiwarter, P. Suntharalingam, E. A. Davidson, P. Ciais, R. B. Jackson, G. Janssens-Maenhout, M. J. Prather, P. Regnier, N. Pan, S. Pan, G. P. Peters, H. Shi, F. N. Tubiello, S. Zaehle, F. Zhou, A. Arneth, G. Battaglia, S. Berthet, L. Bopp, A. F. Bouwman, E. T. Buitenhuis, J. Chang, M. P. Chipperfield, S. R. S. Dangal, E. Dlugokencky, J. W. Elkins, B. D. Eyre, B. Fu, B. Hall, A. Ito, F. Joos, P. B. Krummel, A. Landolfi, G. G. Laruelle, R. Lauerwald, W. Li, S. Lienert, T. Maavara, M. MacLeod, D. B. Millet, S. Olin, P. K. Patra, R. G. Prinn, P. A. Raymond, D. J. Ruiz, G. R. van der Werf, N. Vuichard, J. Wang, R. F. Weiss, K. C. Wells, C. Wilson, J. Yang and Y. Yao, *Nature*, 2020, **586**, 248–256.

2 A. R. Ravishankara, J. S. Daniel and R. W. Portmann, *Science (80-.).*, 2009, **326**, 123–125.

3 *Drawing Down N2O to Protect Climate and the Ozone Layer: A UNEP synthesis report*, 2013.

4 J. C. López, G. Quijano, T. S. O. Souza, J. M. Estrada, R. Lebrero and R. Muñoz, *Appl. Microbiol. Biotechnol.*, 2013, **97**, 2277–2303.

5 K. Kim, J. Byun, H. Kim, K. S. Lee, H. S. Lee, J. Kim, T. Hyeon, J. J. Kim and J. W. Han, *ACS Catal.*, 2021, **11**, 15089–15097.

6 O. Badr and S. D. Probert, *Appl. Energy*, 1992, **41**, 177–200.

7 M. Strokal and C. Kroeze, *Curr. Opin. Environ. Sustain.*, 2014, **9**, 108–121.

8 M. Konsolakis, *ACS Catal.*, 2015, **5**, 6397–6421.

9 X. Lan, K. W. Thoning and E. J. Dlugokencky, Trends in globally-averaged CH4, N2O, and SF6 determined from NOAA Global Monitoring Laboratory measurements.

10 M. Galle, D. W. Agar and O. Watzenberger, *Chem. Eng. Sci.*, 2001, **56**, 1587–1595.

11 G. Centi and F. Vazzana, *Catal. Today*, 1999, **53**, 683–693.

12 A. Wang, Y. Wang, E. D. Walter, R. K. Kukkadapu, Y. Guo, G. Lu, R. S. Weber, Y. Wang, C. H. F. Peden and F. Gao, *J. Catal.*, 2018, **358**, 199–210.

13 X. Xu, H. Xu, F. Kapteijn and J. A. Moulijn, *Appl. Catal. B Environ.*, 2004, **53**, 265–274.

14 A. Kudo and A. Mine, *J. Electroanal. Chem.*, 1996, **408**, 267–269.

15 M. Kato, M. Okui, S. Taguchi and I. Yagi, *J. Electroanal. Chem.*, 2017, **800**, 46–53.

16 M. Kato, Y. Unuma, M. Okui, Y. Qu, J. Zheng, S. Taguchi, F. Kiguchi, M. Torihata, Y. Gao, N. Hoshi and I. Yagi, *Electrochim. Acta*, 2021, **398**, 139281.

17 A. Kudo and A. Mine, *Appl. Surf. Sci.*, 1997, **121–122**, 538–542.

18 A. Ahmadi, E. Bracey, R. Wyn Evans and G. Attard, *J. Electroanal. Chem.*, 1993, **350**, 297–316.

19 A. Aziznia, A. Bonakdarpour, E. L. Gyenge and C. W. Oloman, *Electrochim. Acta*, 2011, **56**, 5238–5244.

20 H. Ebert, R. Parsons, G. Ritzoulis and T. VanderNoot, *J. Electroanal. Chem.*, 1989, **264**, 181–193.

21 B. Wang and X. Y. Li, *Anal. Chem.*, 1998, **70**, 2181–2187.

22 A. C. Sarker, M. Kato and I. Yagi, *Electrochim. Acta*, 2022, **425**, 140628.

23 M. Kato, M. Okui, S. Taguchi and I. Yagi, *J. Electroanal. Chem.*, 2017, **800**, 46–53.

24 J. Yang, F. Calle-Vallejo, M. Duca and M. T. M. Koper, *ChemCatChem*, 2013, **5**, 1773–1783.

25 J. Yang, Y. Kwon, M. Duca and M. T. M. Koper, *Anal. Chem.*, 2013, **85**, 7645–7649.

26 C. J. Poulsen, C. Tabor and J. D. White, *Science (80-.).*, 2015, **348**, 1238–1241.

27 M. M. Magalhães, J. F. Gomes, G. Tremiliosi-Filho, P. B. S. de Figueiredo, R. B. de Lima and F. Colmati, *J. Appl. Electrochem.*, 2021, **51**, 173–181.

28 R. Choi, S. Il Choi, C. H. Choi, K. M. Nam, S. I. Woo, J. T. Park and S. W. Han, *Chem. - A Eur. J.*, 2013, **19**, 8190–8198.

29 Z. Liu, B. Guo, L. Hong and T. H. Lim, *Electrochem. commun.*, 2006, **8**, 83–90.

30 J. Yang, M. Duca, K. J. P. Schouten and M. T. M. Koper, *J. Electroanal. Chem.*, 2011, **662**, 87–92.

31 B. H. Ko, B. Hasa, H. Shin, Y. Zhao and F. Jiao, *J. Am. Chem. Soc.*, 2022, **144**, 1258–1266.

32 J. Zhang, Y. Mo, M. B. Vukmirovic, R. Klie, K. Sasaki and R. R. Adzic, *J. Phys. Chem. B*, 2004, **108**, 10955–10964.

33 K. Sasaki, H. Naohara, Y. Cai, Y. M. Choi, P. Liu, M. B. Vukmirovic, J. X. Wang and R. R. Adzic, *Angew. Chemie - Int. Ed.*, 2010, **49**, 8602–8607.

34 W. C. Trogler, *Coord. Chem. Rev.*, 1999, **187**, 303–327.

35 R. Sander, *Atmos. Chem. Phys.*, 2015, **15**, 4399–4981.

